ELSEVIER

Journal of Quantitative Spectroscopy & Radiative Transfer 93 (2005) 163–173

Journal of Quantitative Spectroscopy & Radiative Transfer

www.elsevier.com/locate/jqsrt

Radiation transfer through nanoscale apertures

E.X. Jin, X. Xu*

School of Mechanical Engineering, Purdue University, West Lafayette, IN 47906, USA

Received 1 February 2004; accepted 1 July 2004

Abstract

An H-shaped nano-aperture used as a high efficient near-field radiator is demonstrated. The transfer efficiency higher than unity and nanoscale radiation spot can be achieved simultaneously in the near field compared with regular apertures. The radiation enhancement is ascribed to the fundamental electric–magnetic field propagating in the TE_{10} mode concentrated in the gap between the ridges, which provides the electric dipole-liked behavior. The optimal performance of nano-apertures could be fulfilled by proper design of the geometry of the aperture, choosing good conducting metals as the film materials and low refractive substrate. As a demonstration, a super small spot about 20 nm × 18 nm is achieved through the radiation of a nano-aperture with a narrow gap of 12 nm × 8 nm.

Keywords: Radiation; Near Field optics; Nanoscale aperture; Transmission enhancement

1. Introduction

An aperture or opening in a cavity resonator or a conducting plate allows radiation leakage or desired radiation in the required direction in a positive manner. In this kind of aperture radiation systems, the field distribution over the aperture acts as the source of radiation according to Huygens principle. If the aperture is large in size in comparison with wavelength, significant radiation could be produced and propagates in a long distance, for example, electromagnetic horn which transfers radiation from a guiding system. For a sub-wavelength aperture, the radiated

*Corresponding author.
E-mail address: xxu@ecn.purdue.edu (X. Xu).

0022-4073/$ - see front matter
doi:10.1016/j.jqsrt.2004.08.019

fields from the source fields over the aperture nearly cancel at large distance, so the radiation is only located in the near field of the aperture, a distance much less than wavelength. Using sub-wavelength apertures as near-field radiation sources has applications in near-field optical microscopy (NSOM) [1-5] to achieve nanoscale optical resolution, and potentially for near-field nanolithography to fabricate nano-structures, optical data storage to reach ultra-high storage density, heat assisted magnetic recording to provide ultra small heat source, and many other areas where a super resolution radiation source is needed. However, the near-field radiation transfer through regular apertures is typically very low [6-9]. For a circular aperture, the transfer efficiency is proportional to the fourth power of ratio of the aperture size to wavelength, thus large input powers are necessary for significant radiation energy when dealing with regular subwavelength apertures, and low performance/cost ratio will be expected.

In order to obtain both nanoscale resolution and high radiation efficiency, a number of shaped apertures have been proposed, including C-shaped, H-shaped, and bowtie-shaped [10-13]. They can be named as ridge nano-apertures in which the small gap region between the two ridges determines the near-field nanoscale resolution. In the following, the analytical procedure of radiation through a circularly shaped, sub-wavelength hole is first outlined, since the results of this calculation are useful to illustrate the mechanisms of radiation transfer enhancement in ridge nano-apertures, as well as to verify the followed numerical calculations. An H-shaped nano-aperture in a thin metal plate is numerically studied using the finite-difference time-domain (FDTD) method [14,15], and compared with comparable conventional apertures. The full wave 3-D electromagnetic fields inside and in the near-field region of the apertures are obtained through FDTD calculations, which helps to understand the process of light propagation and radiation transfer through these nano-apertures. The electric dipole-liked radiation behavior will be discussed. At last, an ultimate super resolution through a nano-aperture with a narrow gap will be demonstrated.

2. Numerical approach

According to Huygens principle, under the illumination from the top surface of an aperture in a thin conducting plate as shown in Fig. 1, the radiation through the aperture can be computed by

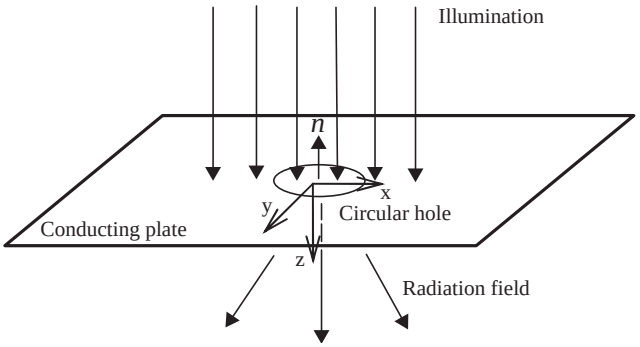

Fig. 1. Schematic view of radiation through a circular hole.

treating the electromagnetic field in the aperture area as the re-radiation source [6,7]. The plate is considered to be perfectly conducting, so that it has no fields or currents on the bottom surface excect in the aperture. Although the field over the aperture arises from the illumination on the top, it may be considered to be produced by equivalent sources located on the aperture top surface, so that an equivalent surface magnetic source M_s can be introduced,

$$\vec{M}_s = \vec{E}_1 \times \vec{n}\,. \tag{1}$$

The original fields $\vec{E}_1$ and $\vec{H}_1$at the top region of the plane are

$$\vec{H}_1 = \vec{H}_0 - \mathrm{j}w\vec{F} - \frac{\mathrm{j}w}{k^2}\nabla(\nabla\cdot\vec{F}), \tag{2a}$$

$$\vec{E}_1 = \vec{E}_0 - \frac{1}{\varepsilon}\nabla\times\vec{F}, \tag{2b}$$

where the vector potential $\vec{F}$ is computed from the equivalent magnetic current $\vec{M}_s$.

$$\vec{F} = \varepsilon\int_s \frac{\vec{M}_s \mathrm{e}^{-\mathrm{j}kr}}{4\pi r}\,\mathrm{d}s. \tag{3}$$

To ensure the continuity of tangential electrical field through the hole, an equivalent magnetic source of $-M_s$ is placed on the bottom surface of the hole. The fields E_2 and H_2 at the bottom region of the plane is equivalent to the fields induced by the magnetic source $-M_s$ and its image,

$$\vec{H}_2 = \mathrm{j}w\vec{F} + \frac{\mathrm{j}w}{k^2}\nabla(\nabla\cdot\vec{F}), \tag{4a}$$

$$\vec{E}_2 = \frac{1}{\varepsilon}\nabla\times\vec{F}\,. \tag{4b}$$

Applying the continuity of the tangential component of the magnetic fields across the hole, the magnetic source M_s is solved using Rayleigh series expansion:

$$\vec{M}_s = \sum_m \vec{M}_s^{\,m} k^m \tag{5}$$

In our case, it is assumed that the normally incident laser beam is a TEM plane wave, as the transverse dimension of the beam is much larger than the diameter of the small hole. The time-harmonic electric and magnetic field (with time dependence $\mathrm{e}^{\mathrm{j}wt}$) of the incident beam are expressed as

$$\vec{E}_0 = E_0\mathrm{e}^{-\mathrm{j}kz}\vec{x}, \tag{6a}$$

$$\vec{H}_0 = H_0\mathrm{e}^{-\mathrm{j}kz}\vec{y}\,. \tag{6b}$$

As such, the low-frequency expansion of Eq. (5) up to the k^2 term is found as

$$M_{s\rho} = \frac{8\mathrm{j}}{3\pi}E_0\sin\theta(a^2-\rho^2)^{1/2}k + o(k^3), \tag{7a}$$

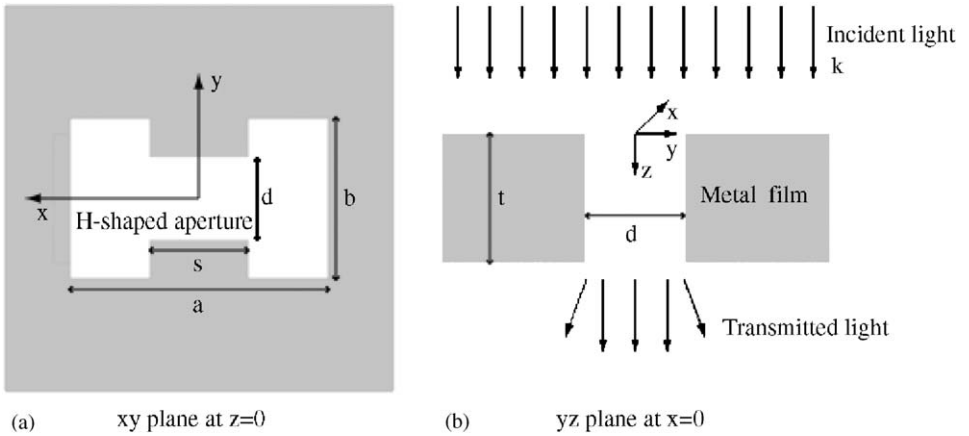

Fig. 2. (a and b) Schematic view of an H-shaped nano-aperture channel in a free-standing metal film.

$$M_{s\theta} = \frac{4j}{3\pi} E_0 \cos\theta \frac{2a^2 - \rho^2}{(a^2 - \rho^2)^{1/2} k} + o(k^3), \tag{7b}$$

$$\vec{M}_s = M_{s\rho}\,\vec{\rho} + M_{s\theta}\,\vec{\theta}, \tag{7c}$$

where a is the radius of the hole. With the magnetic source term determined, the radiated field below the hole can be completely solved, as well as the time-averaged radiation transfer through the hole.

For apertures with other geometry, such as shown in Fig. 2, an H-shaped ridge nano-aperture, it is difficult to analytically determine the equivalent magnetic current sources, and therefore numerical computations are necessary. The Maxwell's differential equations for the light propagation and radiation transfer are solved numerically with 3D-FDTD method. The radiation fields are calculated by solving the discretized Maxwell curl equations in both space and time for each time step until the steady state is reached. In the case of a sinusoidal illumination as used in this work, the sinusoidal variation of all radiated fields in time indicates the achievement of steady state. At optical frequencies the modified Drude model [15] is used to describe the frequency dependence of the complex relative permittivity of real metals.

3. Results and discussion

Radiation through a small hole of 50 nm in diameter under the illumination of a plane wave of 500 nm in wavelength is computed based on the analysis described above. Figs. 3(a) and (b) give the variation of electric and magnetic fields on the central axis of the hole with the distance (z/d) away from the hole. The normalized electric field E/E_0 and magnetic field H/H_0 in the near field are about 10^{-2}, which is in agreement with Bethe's result [6] of the order of $(a/\lambda)^2$. The radiation is mainly concentrated in the near-field region of the hole, i.e., the diameter of the hole rather than

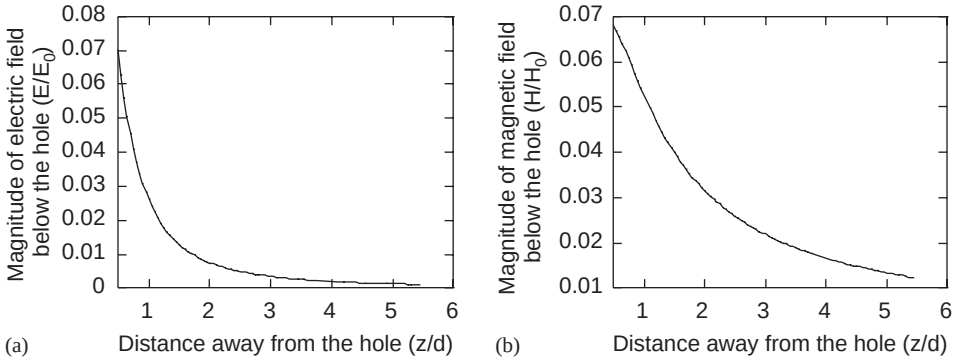

Fig. 3. Variation of electric (a) and magnetic field (b) with the distance from the circular aperture.

the wavelength. In our case, the transfer efficiency is about the order of 10^{-3}–10^{-4}, which also agrees with the Bethe's result of $(a/\lambda)^4$. FDTD numerical procedures are verified by computing the same case illustrated in Fig. 3, and the same results are obtained in terms of radiation fields and transfer efficiency.

To demonstrate the field enhancement in the H-shaped aperture, numerical calculations are carried out to compare the ridge aperture with two regular apertures, a 300 nm × 200 nm rectangular aperture and a 100 nm × 100 nm square aperture. Fig. 4 shows distributions of electric field intensity $|E|^2$ for the three apertures on the xz plane at $y = 0$ and xy plane 50 nm below the apertures after reaching steady states in the case of y-polarized 488 nm uniform illumination from the top region. A 100 nm thick ideal conductor plate is considered in these calculations since the optical absorption depth for most real metals are only a few nanometers. Due to the finite thickness of the aperture, it could be treated as a short aperture waveguide without considering the end effect. The current induced on the far side surface is negligible therefore the aperture is the only re-radiating source. As the cutoff wavelength of the square aperture is far below the incident wavelength, it is basically a cutoff waveguide and no propagating waveguide mode can exist inside the aperture, so there is much less radiation energy through the aperture. In contrary, the cutoff wavelengths of TE_{10} propagation mode in the rectangular and H-shaped apertures are 600 and 805 nm, respectively, therefore significant near-field radiations are expected as shown in Fig. 4(b) and (a). The cutoff of the H-shaped aperture is calculated by using the transverse resonance method in microwave engineering and the geometry considered in this work ($a = 300$ nm, $b = 200$ nm, $s = 100$ nm, $d = 100$ nm as shown in Fig. 2). Due to the cutoff effect, the radiation transfer of the evanescent wave through the square aperture channel is as low as 0.0038, while the radiation efficiency through the H-shaped aperture is 2.14, which means the H-shaped aperture can provide about three orders improvement in radiation transfer compared to the square aperture. Furthermore, the H-shaped aperture shows a much smaller near-field radiation spot with respect to the rectangular aperture while maintaining the comparable peak radiation intensity as shown in Fig. 4(d) and (e).

Further numerical calculations are conducted to illustrate the mechanism of light propagation and radiation transfer through ridge aperture. The geometry of the H-shaped aperture is same as mentioned before, but the film thickness considered here is 500 nm in order to show the

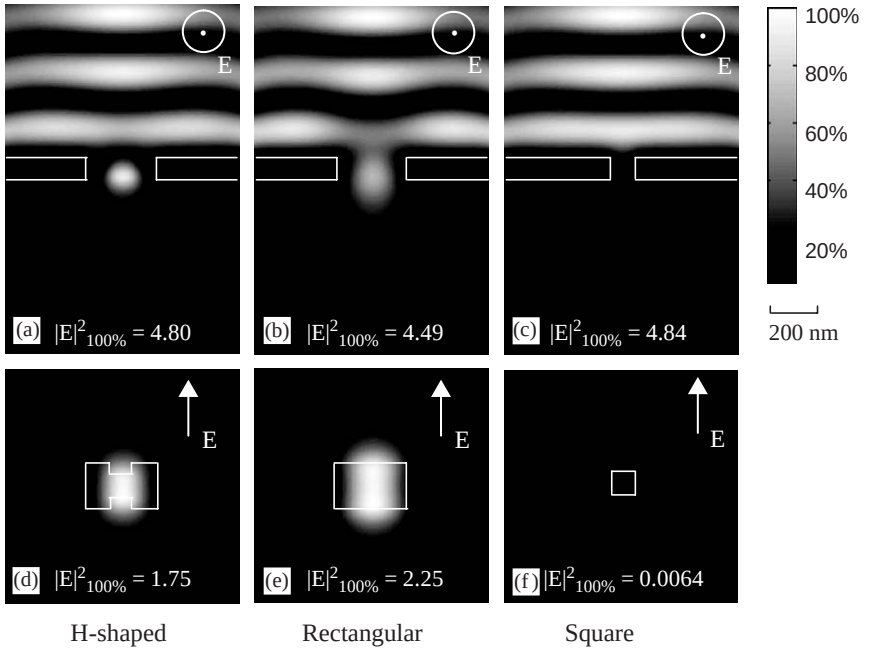

Fig. 4. (a–f) Electric field intensity $|E|^2/|E_0|^2$ distribution of H-shaped, rectangular and square nano-apertures. The first and second rows show the xz plane at $y=0$ and xy plane 50 nm below the aperture, respectively.

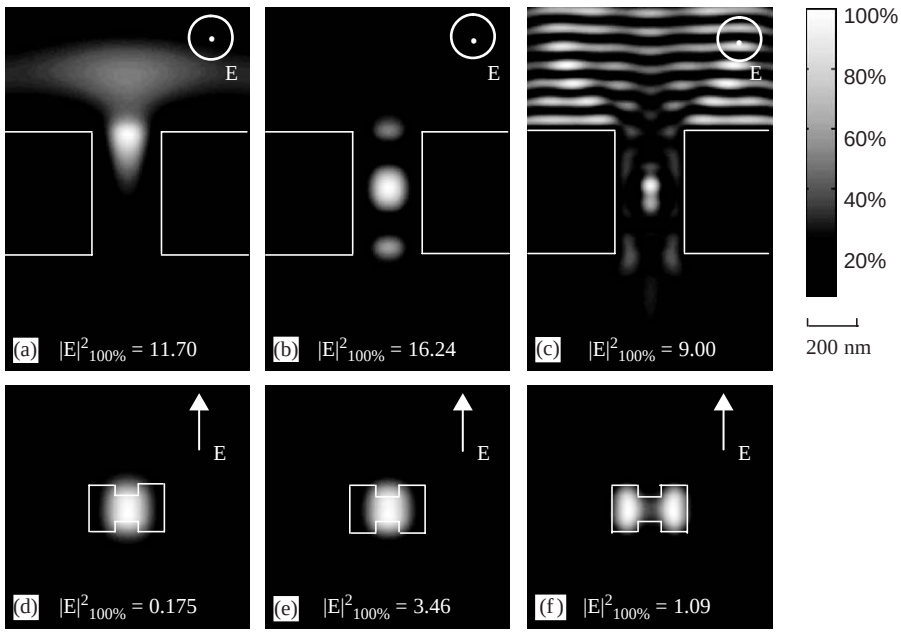

Fig. 5. (a–f) Electric field intensity $|E|^2/|E_0|^2$ distribution of an H-shaped aperture in a 500 nm perfect conducting film on xz plane at $y=0$ and xy plane 50 nm below the aperture in the first and the second row, respectively. Y-polarized incident plane wave of different wavelengths is considered. From the first to third column, the wavelength is 1000, 500, and 150 nm, respectively.

propagation modes inside the aperture channel. Electric field intensity are calculated and displayed in Fig. 5 with y-polarized illumination of three different wavelengths, 1000, 500 and 150 nm.In the case of 1000 nm incident illumination, only the evanescent mode whose intensity decays rapidly along the aperture due to the cutoff effect is clearly shown in Fig. 5(a), and low radiation through the aperture is expected. At 500 nm incident wavelength, which is shorter than the cutoff wavelength, the TE_{10} waveguide mode is observed in the aperture channel (Fig. 5(b)). It is found that this mode is completely confined in the gap region between the two ridges and it maintains the confinement even beyond the aperture as shown in Fig. 5(e). Since TE_{10} is a propagating waveguide mode, high radiation intensity through the aperture is achieved opposite to the exponential decay of radiation intensity in the evanescent case. However, the fundamental TE_{10} mode is not the only propagation mode that can be excited. When illuminated with 150 nm incidence, a TE_{20} mode is also excited in the aperture (Fig. 5(c)), which propagates through the side open regions of the aperture and dominates the field even at 50 nm below the aperture (Fig. 5(f)), therefore optical confinement is not achieved.

The calculation results also show that the H-shaped aperture functions as an electric dipole radiator. The profile of radiation power densities on the plane right below the H-shaped aperture in Fig. 6 shows that the radiation is dominated by the electric field in the near field of the aperture. This is in contrast to the sub-wavelength circular hole, in which the electric field decays much faster than the magnetic field does in the near-field region as shown in Fig. 3. In order to illustrate this point further, radiation transfer through a square aperture is also calculated numerically. It is seen that the radiation power density is dominated by the magnetic field as shown in Fig. 7, which shows the radiation function of a magnetic dipole. It should be noted that in terms of optical applications, e.g., nanolithography, the electric dipole-liked radiation behavior of the ridge apertures offers advantage over the regular apertures since the interaction of visible light with media, for example, photo resist, is dominated by the electric field.

At optical frequencies, real metals have finite skin depth, which cannot be neglected in a thin film. Furthermore, the negative value of the real part of complex dielectric constant for most

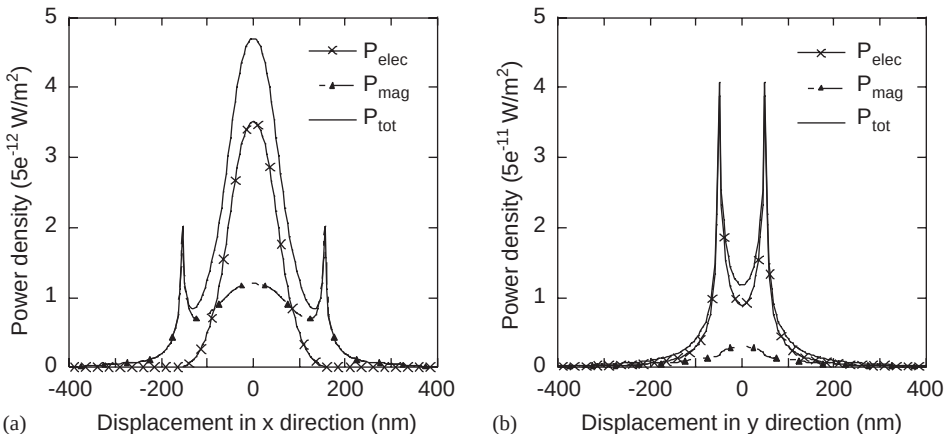

Fig. 6. (a and b) Radiation power density profiles of an H-shaped aperture. The magnitude of incident electric field is 1 V/m.

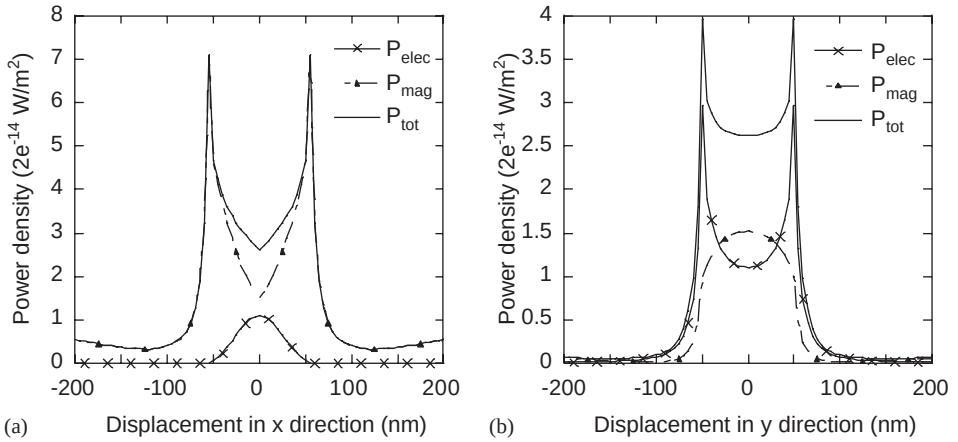

Fig. 7. (a and b) Radiation power density profiles of a 100 nm × 100 nm square aperture. The magnitude of incident electric field is 1 V/m.

metals will give rise to the excitation of surface plasmon since the surface plasmon dispersion relation can be satisfied at the interface of metal film and free space [16]. To investigate the effect of surface plasmon, an H-shaped aperture ($a = 300$ nm, $b = 120$ nm, $s = 100$ nm and $d = 50$ nm) in 50 nm films made of aluminum and silver are studied. The incident wavelength is chosen to be 488 nm. Fig. 8 shows radiation intensity distributions in the vicinity of the apertures. The field intensity is strongly localized on the edges of the aperture in the silver film (Fig. 8(b)), and it indicates the excitation of coherent oscillation of accumulated electron charges at these locations, or localized surface plasmon (LSP). The LSP will propagate along the silver/air interface but decay exponentially in the direction perpendicular to the aperture. Due to the fact that the absolute value of the ratio of the real part of the dielectric constant to the imaginary part for silver is larger than that for aluminum [16], surface plasmon excitation is much stronger for silver than for aluminum. It has been shown the surface plasmon enhances the transmission through a hole array in silver film [17,18], but the localized surface plasmon excitation here has a negative effect on the field confinement as evident in Fig. 8(d). In contrary, the fact that the radiation spot in the aluminum keeps focused suggests that aluminum can be treated as an ideal conduct under 488 nm illumination, which does not allow for the excitation of free electrons on the bottom surface.

Another issue needs to be considered in practical applications is the effect of substrate on which the metal film is deposited. Fig. 9 shows radiation field intensity at distance 50 nm behind the H-shaped aperture on a free-standing aluminum film or the same film sitting on a substrate (dielectric constant $\varepsilon = 4.2$). The aperture has the same geometry as discussed in Fig. 8. The peak electric field intensity is reduced and the full width half magnitude (FWHM) of field intensity increases both in the x and y directions in the case of substrate $\varepsilon = 4.2$ as shown in Fig. 9. Due to the existence of substrate, the relative incident wavelength is reduced from λ to λ/n (n is the refractive index of the substrate), which is closer to the cutoff wavelength of T_{20} mode in the cutoff spectrum. As shown in Fig. 5 before, light will transport through the side regions of the aperture channel when T_{20} mode is excited, and the H-shaped aperture will lose its ability to concentrate radiation.

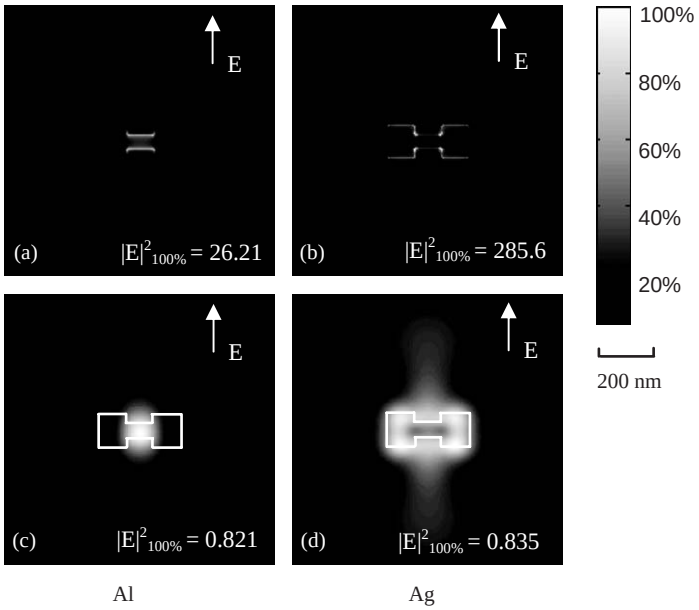

Fig. 8. (a–d) Normalized radiation field intensity of an H-shaped aperture in a 50 nm thick aluminum and silver film. The first row is the *xy* plane right below the film and the second row is 50 nm below the film.

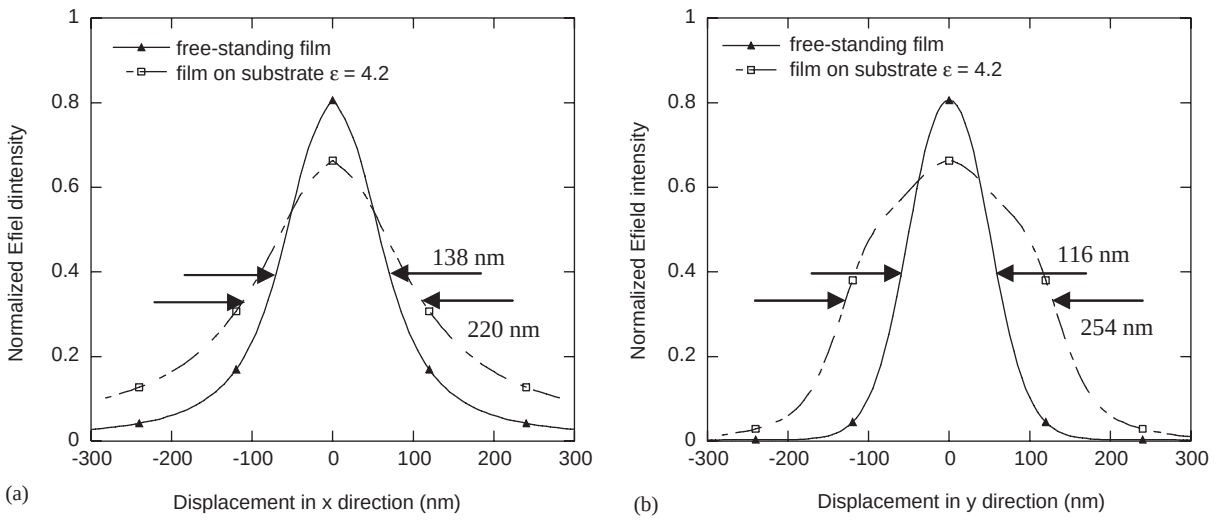

Fig. 9. Profiles of normalized radiation field intensity at distance 50 nm below an H-shaped aperture on a free-standing aluminum film or the same film sitting on a substrate in x (a) and y (b) directions.

Based on the above calculations, it can be said that in order to obtain the optimal radiation performance, i.e., high-radiation efficiency and excellent radiation confinement of an H-shaped nano-aperture, first, good conducting and plasmon-free metals such as aluminum need to be

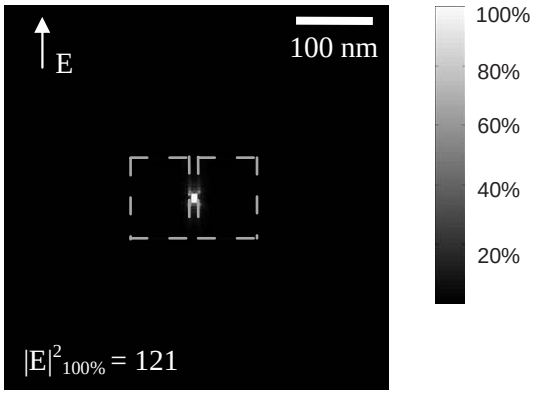

Fig. 10. Normalized radiation field intensity 4 nm below an H-shaped aperture with a narrow gap in a 50 nm thick aluminum film under 488 nm polarized illumination. An ultra small spot 20×18 nm is confined in the center.

chosen as the film material to reduce the negative LSP effect. Second, transparent material with low refractive index should be considered as the substrate to maintain the radiation confinement. Finally, the geometry of the aperture must be well designed to fit the excitation frequency between the cutoff frequencies of TE_{10} mode and TE_{20} mode so that only the TE_{10} propagation mode can be excited in the aperture. The small gap formed by the ridges confines the light and determines the size of the nanoscale radiation spot. As a demonstration, an ultra small (20 nm × 18 nm) and high intensity radiation spot is illustrated in Fig. 10. This ultra small spot is obtained at a distance 4 nm below an H-shaped aperture in a 50 nm thick aluminum film, with a narrow gap of 12 nm × 8 nm and irradiated by 488 nm polarized light.

4. Conclusions

H-shaped nano-apertures can be used as a near-field radiation source to achieve nanoscale resolution with high transmission efficiency and high contrast compared with regular shaped nano-apertures. The propagation of fundamental TE_{10} mode formed between the ridges contributes to the field enhancement and concentration. With careful selections of the materials for metal film and substrate, and optimal design of the geometry of ridge nano-aperture, a small radiation source with high intensity could be obtained, which will be very attractive in the applications such as ultra high optical data storage. In the next stage, NSOM experiments will be conducted to characterize radiation through nano-apertures.

Acknowledgements

Support to this work by the National Science Foundation is acknowledged.

References

[1] Synge EH. A suggested method for extending the microscopic resolution into the ultramicroscopic region. Philos Mag 1928;6:356–8.
[2] Ash EA, Nicholls G. Super-resolution aperture scanning microscope. Nature 1972;237:510–2.
[3] Pohl DW, Denk W, Lanz M. Optical stethoscopy: image recording with resolution $\lambda/20$. Appl Phys Lett 1984;44:651–3.
[4] Lewis A, Isaacson M, Harootunian A, Muray A. Development of a 500 Å spatial resolution light microscope. Ultramicroscopy 1984;13:227–32.
[5] Fischer UC. Optical characteristics of 1.0 μm circular apertures in a metal film as light sources for scanning ultramicroscopy. J Vac Sci Technol B 1985;3:386–90.
[6] Bethe HA. Theory of diffraction by small holes. Phys Rev 1944;66:163–82.
[7] Bouwkamp CJ. On Bethe's theory of diffraction by small holes. Philips Res Rep 1950;5:321–32.
[8] Leviatan Y. Study of near-zone fields of a small aperture. J Appl Phys 1986;60:1577–83.
[9] Roberts A. Near-zone fields behind circular apertures in thick, perfectly conducting screens. J Appl Phys 1989;65:2896–9.
[10] Shi X, Hesselink L. Mechanisms for enhancing power throughput from planar nano-apertures for near-field optical data storage. Jpn J Appl Phys 2002;41:1632–5.
[11] Shi X, Hesselink L, Thornton RL. Ultrahigh light transmission through a C-shaped nanoaperture, Optics Lett 2003;28:1320–2.
[12] Itagi AV, Stancil DD, Bain JA, Schlesinger TE. Ridge waveguide as a near-field optical source. Appl Phys Lett 2003;83:4474–6.
[13] Jin EX, Xu X. Finite-difference time-domain studies on optical transmission through planar nano-apertures in a metal film. Jpn J Appl Phys 2004;43:407–17.
[14] Yee KS. Numerical solution of initial boundary value problems involving Maxwell's equations in isotropic media. IEEE Trans Antennas Propag 1966;14:302–7.
[15] Kunz K, Luebbers R. The finite difference time domain method for electromagnetics. Boca Raton: CRC Press; 1996.
[16] Raether H. Surface plasmons on smooth and rough surfaces and on gratings. Berlin: Springer; 1988.
[17] Ebbesen TW, Lezec HJ, Ghaemi HF, Thio T, Wolff PA. Extraordinary optical transmission through sub-wavelength hole arrays. Nature 1998;391:667–9.
[18] Ghaemi HF, Thio T, Grupp DE, Ebbesen TW, Lezec HJ. Surface plasmon enhance optical transmission through subwavelength holes. Phys Rev B 1998;58:6779–82.